

# The 2175 Å Interstellar Extinction Bump: Is the Wavelength Variable?

Qian Wang<sup>1,2</sup>, X.J. Yang<sup>1,2\*</sup>, and Aigen Li<sup>2†</sup>

<sup>1</sup>Hunan Key Laboratory for Stellar and Interstellar Physics and School of Physics and Optoelectronics, Xiangtan University, Hunan 411105, China

<sup>2</sup>Department of Physics and Astronomy, University of Missouri, Columbia, MO 65211, USA

## ABSTRACT

The most striking characteristics of the mysterious 2175 Å extinction bump, the strongest spectroscopic absorption feature seen on the interstellar extinction curve, are the invariant central wavelength and variable bandwidth: its peak position at 2175 Å is remarkably constant while its bandwidth varies from one line of sight to another. However, recent studies of the lines of sight toward a number of Herbig Ae/Be stars have revealed that the extinction bump exhibits substantial shifts from the canonical wavelength of 2175 Å. In this work we revisit these lines of sight and take a physical approach to determine the ultraviolet (UV) extinction curve for each line of sight. It is found that the wavelengths of the derived UV extinction bumps are around 2200 Å and the scatters are considerably smaller than that of the previous study based on the same set of Herbig Ae/Be stars, consistent with the conventional wisdom. Nevertheless, the scatters are still appreciably larger than that associated with the nominal bump position of 2175 Å. This is discussed in the context that Herbig Ae/Be stars are not well-suited for interstellar extinction studies.

**Key words:** ISM: dust, extinction — ISM: lines and bands — ISM: molecules

## 1 INTRODUCTION

The 2175 Å extinction bump was first detected nearly six decades ago by Stecher (1965). It shows up as the most prominent spectral feature on the interstellar extinction curve. It is widely seen in the Milky Way and nearby galaxies, including the Large Magellanic Cloud, several regions in the Small Magellanic Cloud, and M31 (see Whittet 2022). Very recently, it was detected by the *James Webb Space Telescope* (JWST) in a distant galaxy at redshift  $z \approx 6.71$  (Witstok et al. 2023).

Despite nearly 60 years' extensive observational, theoretical and experimental studies, the exact carrier of the 2175 Å extinction bump remains unidentified, although various candidate materials have been proposed, including small graphitic grains (Stecher & Donn 1965, Draine 1988), polycyclic aromatic hydrocarbon (PAH; Joblin et al. 1992, Li & Draine 2001, Steglich et al. 2013), and carbon buckyonions composed of spherical concentric fullerene shells (Chhowalla et al. 2003, Iglesias-Groth et al. 2003, Ruiz et al. 2005, Li et al. 2008). More recently, Ma et al. (2020) found that a new carbon allotrope known as T-carbon, formed by substituting

each atom in diamond with a carbon tetrahedron (Sheng et al. 2011), exhibits a prominent peak around 2175 Å in its electronic absorption spectrum.

The difficulty in identifying the carrier of the 2175 Å extinction bump is mainly related to its striking characteristics: while its strength and width vary with environment, its peak position is quite invariant: the central wavelength of this feature varies by only  $\pm 0.46\%$  ( $2\sigma$ ) around 2175 Å ( $4.6 \mu\text{m}^{-1}$ ), while its full width half maximum (FWHM) varies by  $\pm 12\%$  ( $2\sigma$ ) around 469 Å ( $\approx 1 \mu\text{m}^{-1}$ ). The bump width appears to show a strong correlation with the environment. In general, broad bumps are often seen in dense, quiescent environments, while narrower bumps are mainly seen in diffuse regions and regions of recent early-type star formation (Fitzpatrick & Massa 1986; hereafter FM86). There is no substance that can explain the observational fact that the central wavelength of the 2175 Å extinction bump basically does not change with the environment. For example, although increasing the size of graphite grains can broaden the bump, its peak shifts to longer wavelength which is inconsistent with the observational characteristic of a stable peak wavelength (Draine & Malhotra 1993, Mathis 1994).

Recently, Blasberger et al. (2017) analyzed the UV spectra of 26 Herbig Ae/Be (HAeBe) stars obtained with the *International Ultraviolet Explorer* (IUE) and determined the

\* xjyang@xtu.edu.cn

† lia@missouri.edu

UV extinction curves for the lines of sight toward these stars. Contrary to the conventional wisdom, the extinction bumps derived by Blasberger et al. (2017) do not always peak at 2175 Å. Instead, they exhibit significant shifts of the central wavelength of the extinction bump. If confirmed, this would be an important breakthrough in the interstellar extinction studies, particularly, this will provide valuable insight into the carriers of the 2175 Å bump. This motivates us to revisit all these 26 sight lines. In §2 we briefly describe the sample and method. The results are presented and discussed in §3. Our major conclusion is summarized in §4.

## 2 THE SAMPLE AND METHOD

We consider the sample of Blasberger et al. (2017), which consists of 26 pre-main-sequence stars of spectral type A2 and earlier. All have significant UV absorption (equivalent width,  $EW \gtrsim 100$  Å) around 2175 Å. The sample and the stellar parameters are listed in Table 1.

Following Blasberger et al. (2017), we derive the UV extinction curve for each line of sight by comparing  $F_{\lambda}^{\text{obs}}$ , the stellar spectrum observed by the IUE which suffers dust extinction, with  $F_{\lambda}^{\text{int}}$ , the *intrinsic* stellar spectrum which is free of dust extinction. The IUE spectra were extracted from the *Mikulski Archive for Space Telescopes*,<sup>1</sup> by combining data obtained with three cameras: the short-wavelength camera (SWP) which spans the wavelength range of 1200–1970 Å, and the two long-wavelength cameras (LWP and LWR) which span the wavelength range of 1970–3200 Å.

We approximate the intrinsic stellar spectrum by the stellar model atmospheric spectrum of Castelli & Kurucz (2004).<sup>2</sup> Let  $A_{\lambda}$  be the extinction at wavelength  $\lambda$ , and  $A_V$  be the visual extinction. The observed IUE spectrum and the intrinsic stellar spectrum are related through dust extinction

$$F_{\lambda}^{\text{obs}} = F_{\lambda}^{\text{int}} \exp\left(-\frac{A_{\lambda}}{A_V} \frac{A_V}{1.086}\right). \quad (1)$$

Let  $F_{\nu}^{\text{RK}}$  be the Kurucz model atmospheric flux at stellar surface (in unit of  $\text{erg s}^{-1} \text{cm}^{-2} \text{Hz}^{-1}$ ). At an Earth-stellar distance of  $d$ , the intrinsic, extinction-free flux (in unit of  $\text{erg s}^{-1} \text{cm}^{-3}$ ) would be

$$F_{\lambda}^{\text{int}} = F_{\nu}^{\text{RK}} \times \frac{c}{\lambda^2} \times \left(\frac{R_{\star}}{d}\right)^2, \quad (2)$$

where  $c$  is the speed of light.

Following Fitzpatrick & Massa (1988; hereafter FM88) and Cardelli et al. (1989), we represent the wavelength-dependence of extinction by an analytical formula consisting of three parts,

$$\frac{A_{\lambda}}{A_V} = c_1 + c_2x + c_3D(x; \gamma, x_0) + c_4F(x), \quad (3)$$

where  $x \equiv \lambda^{-1}$  is the inverse wavelength;  $c_1 + c_2x$  is the linear background;  $D(x; \gamma, x_0)$ , a Drude function of width  $\gamma$  (in unit of  $\mu\text{m}^{-1}$ ) peaking at  $x_0$  (also in unit of  $\mu\text{m}^{-1}$ ), characterizes the 2175 Å extinction bump and is defined as

$$D(x; \gamma, x_0) = \frac{x^2}{(x^2 - x_0^2)^2 + x^2\gamma^2}, \quad (4)$$

and  $F(x)$  is the far-UV (FUV) nonlinear rise at  $x > 5.9 \mu\text{m}^{-1}$  as described by

$$F(x) = \begin{cases} 0.5392(x - 5.9)^2 + 0.05644(x - 5.9)^3 & x \geq 5.9 \mu\text{m}^{-1}, \\ 0 & x < 5.9 \mu\text{m}^{-1}. \end{cases} \quad (5)$$

The Castelli & Kurucz (2004) stellar atmospheric model is characterized by four parameters: effective temperature  $T_{\text{eff}}$ , gravity  $\log g$ , metal abundance  $[\text{M}/\text{H}]$ , and microturbulence  $\xi$ . The Castelli & Kurucz (2004) stellar model spectral library spans a range in  $T_{\text{eff}}$  from 35,000 K to 50,000 K,  $[\text{M}/\text{H}] = -1.5, -1.0, -0.5, 0.0$ , and 0.5 (relative to solar abundance),  $\log g$  from 0.0 dex to 5.0 dex, and  $\xi = 2.0 \text{ km s}^{-1}$ . For a source of given spectral type (therefore  $T_{\text{eff}}$ ), to select the most appropriate stellar model atmospheric spectrum, we try all the possible metallicities and gravities and select those that best fit the measured spectrum.

For each object, we make use of the Levenberg–Marquardt algorithm to fit the observed spectrum (see eq. 1) by minimizing  $\chi^2$ . The best-fit parameters  $A_V$ ,  $\gamma$ ,  $x_0$ ,  $c_1$ ,  $c_2$ ,  $c_3$ , and  $c_4$  are listed in Table 2. During the fitting process, we find that the bump width  $\gamma$  and peak position  $x_0$  are relatively independent of the other parameters and can be accurately determined. Therefore, we first fix  $\gamma$  and  $x_0$  and fit the observed IUE spectrum to search for best-fitting  $c_1$ ,  $c_2$  and  $c_4$ . We then fix  $\gamma$ ,  $x_0$ ,  $c_1$ ,  $c_2$  and  $c_4$  and re-fit the observed spectrum to determine  $c_3$  and  $A_V$ . Finally, we take these values as initial “guesses” and fit the observed spectrum again so that we derive a full set of model parameters (i.e.,  $A_V$ ,  $c_1$ ,  $c_2$ ,  $\gamma$ ,  $x_0$ ,  $c_3$ , and  $c_4$ ). We repeat this last step three times so that we achieve the minimum  $\chi^2$ .

## 3 RESULTS AND DISCUSSION

For each object, we show in Figures 1–6 the observed IUE spectrum ( $F_{\lambda}^{\text{obs}}$ ) in comparison with the Kurucz model-based, extinction-free “intrinsic” spectrum ( $F_{\lambda}^{\text{int}}$ ), and with the best-fit, dust-obscured Kurucz model spectrum ( $F_{\lambda}^{\text{int}} \exp\{-A_{\lambda}/1.086\}$ ). Also shown are, for each line of sight, the derived extinction curve and its three components, i.e., the linear background, the 2175 Å bump, and the FUV rise.

Figures 1–6 demonstrate that our approach is successful in closely reproducing the observed IUE spectra in the wavelength range of  $\sim 1200$ – $3200$  Å for 25 (of 26) sources. The only exception is HD 95881. As shown in Figure 6, our approach could not fit the observed IUE spectrum in the wavelength range of  $\sim 1200$ – $3200$  Å. Our model spectrum at  $\sim 1600$ – $2000$  Å appreciably exceeds the observed IUE spectrum. Nevertheless, if we confine ourselves to 1600–3200 Å, our model has no problem in closely explaining the observed spectrum. We have also tried to fit the IUE spectra of all other 25 sources *exclusively* in the 1600–3200 Å wavelength range. It is found that the derived peak wavelength and width of the extinction bump are essentially the same as that derived from fitting the IUE spectra over the entire 1200–3200 Å wavelength range (see Table 2).

We show in Figure 7 the histogram of the central wavelengths ( $\lambda_0$ ) of the 2175 Å extinction bump derived for all 26 sources. Except for HD 95881 for which  $\lambda_0$  is derived from

<sup>1</sup> <https://archive.stsci.edu/iue/>

<sup>2</sup> <http://kurucz.harvard.edu/grids/gridxxodfnew>

fitting the IUE spectrum over  $\sim 1600\text{--}2000$  Å, for all other 25 sources, we determine  $\lambda_0$  from the IUE spectra over  $1200\text{--}3200$  Å. Figure 7 reveals that the peak wavelengths of the extinction bump of our sample of 26 sources cluster around  $2200$  Å, with a standard deviation of only  $\sim 33$  Å. The line of sight toward HD 100546, with  $\lambda_0 \approx 2299$  Å, has the longest peak wavelength. If we exclude HD 100546, the median peak wavelength of our sample becomes  $\lambda_0 \approx 2201 \pm 27$  Å. Figure 7 demonstrates that although the bumps of our sample peak at relatively longer wavelengths, their peak wavelengths are rather stable and the scatters are small. Compared with that derived by Blasberger et al. (2017), the peak wavelengths derived here are appreciably less scattered.

To determine the peak wavelengths of the extinction bump of these sources, Blasberger et al. (2017) took an approach differing from ours. They fitted the IUE spectra around the  $2175$  Å extinction bump in the wavelength range of  $1600\text{--}3200$  Å. They took the Castelli & Kurucz (2004) model atmospheric spectrum ( $F_\nu^{\text{RK}}$ ), modulated by a power law to represent the broadband extinction, and absorbed by a feature with a Drude profile. They assumed the measured flux spectrum  $F_\lambda^{\text{obs}}$  as a function of wavelength  $\lambda$  to take the following form:

$$F_\lambda^{\text{obs}} = F_\nu^{\text{RK}} \times N \times \left( \frac{\lambda}{2000\text{Å}} \right)^{-\alpha} \times \exp \left( \frac{-A}{\pi} \frac{\lambda^2}{(\lambda^2 - \lambda_0^2) + \lambda^2 w^2} \right), \quad (6)$$

where  $N$  is the normalization factor,  $\alpha$  is the power law slope, and in the exponent,  $A$  represents the amplitude of the absorption feature,  $w$  its width, and  $\lambda_0$  its central wavelength. Comparing the approach of Blasberger et al. (2017) with ours (see eq. 1), it is apparent that the major difference is that they assumed the attenuation caused by the broadband extinction (i.e., the linear background extinction component  $c_1 + c_2 \lambda^{-1}$ ) take a power-law form  $\lambda^{-\alpha}$ , while we take a physical approach in which the attenuation caused by the linear background extinction is  $\exp \{-c_1 + c_2 \lambda^{-1}\}$ . Apparently, it has to be justified if the power-law  $\lambda^{-\alpha}$  is a valid approximation of the attenuation  $\exp \{-c_1 + c_2 \lambda^{-1}\}$ . In Figure 8 we compare the peak wavelengths of the extinction bumps derived here with that of Blasberger et al. (2017). Clearly, the peak wavelengths derived by Blasberger et al. (2017) were systematically longer than that derived here from a more physical approach.

We argue that, based on a physical fitting of the observed IUE spectra of 26 interstellar lines of sight, the peak wavelengths of the extinction bump are more or less stable around  $\sim 2200$  Å, although they are longer than the nominal  $2175$  Å. We note that, very recently, an extinction bump peaking at  $\sim 2263^{+20}_{-24}$  Å was discovered by JWST in JADES-GS+53.15138-27.81917, a galaxy at  $z \approx 6.71$  (Witstok et al. 2023). This is notably longer than the nominal  $2175$  Å. Draine & Malhotra (1993) have investigated the effects on the  $2175$  Å extinction bump of changes in graphite size and shape. They found that, while small graphite grains do produce a pronounced extinction bump, the central wavelength of the bump is correlated with the bump width. In Figure 9 we compare the central wavelengths with the widths of the extinction bumps derived here. Contrary to Draine & Malhotra (1993), no correlation is found. This is in agreement with Fitzpatrick & Massa (1986) who found large variations

in width of the extinction bump with minimal, and uncorrelated, variations in the central wavelength.

Finally, we note that, although the extinction bump positions derived here are considerably less scattered than that of Blasberger et al. (2017), they are still appreciably more scattered than that of the classical studies. Fitzpatrick & Massa (1986) studied the IUE data of 45 stars and derived a stable bump peak of  $\sim 2174.4$  Å and a  $2\sigma$  scatter of  $\sim 10$  Å. Based on the IUE data of 417 stars, Valencic et al. (2004) placed the peak of the extinction bump at  $\sim 2179$  Å with a  $1\sigma$  scatter of only  $\sim 5$  Å. The discrepancy between the present work and that by Fitzpatrick & Massa (1986) and Valencic et al. (2004) may arise from the validity of HAEBe stars as an interstellar extinction indicator. It is well recognized that HAEBe stars are surrounded by circumstellar disks. Free-free emission from these disks extends well into the V-band, thus adding to the measured  $E(B - V)$  value normally attributed to interstellar reddening (e.g., see Garrison 1978, Schild 1978, Witt & Cottrell 1980).

Furthermore, HAEBe stars are frequently embedded in nebulosity. When they are used for extinction studies, scattered nebular continuum could enter the relatively large apertures ( $\sim 10'' \times 20''$ ) of the IUE spectrometers, adding to the apparent stellar flux and changing the stellar spectral energy distribution (SED); also, a substantial fraction of the dust-related extinction may arise in the nebulosity itself, where the dust properties may not be representative of typical interstellar dust. It is not entirely clear why the nebulosity and the local extinction in the vicinity of HAEBe stars cause the bump positions to systematically shift to longer wavelengths. We argue that this is probably related to the non-standard scattering and extinction properties of the local (i.e., nebular and circumstellar) dust. Due to grain growth, the nebular and circumstellar dust grains around HAEBe stars are generally much larger than interstellar grains (e.g., see Li & Lunine 2003) and therefore they cause less obscuration in the UV. This would effectively raise the flux level observed at shorter wavelengths and therefore cause the bump to shift to longer wavelengths.

Moreover, depending on the geometries and orientations of the circumstellar disks surrounding those HAEBe stars, the observed SEDs of the stars may suffer additional changes due to absorption in the disk. In particular, unresolved (at IUE resolution) absorptions in Fe II/Fe III multiplets arising in the disk can alter the apparent SEDs of HAEBe stars in the  $\sim 2000\text{--}3500$  Å wavelength region, potentially affecting the appearance of the  $2175$  Å extinction bump.

Finally, many HAEBe stars are actively accreting material from the circumstellar disk. Accretion shocks from the infalling material impacting on the stellar photosphere can give rise to UV excess radiation that is more readily observed in cooler accreting stars but which can also alter the intrinsic photospheric SEDs of hotter stars.

In view of these caveats of HAEBe stars as an effective indicator for interstellar extinction, the discovery of variable peak positions by Blasberger et al. (2017) for the  $2175$  Å extinction bump is questionable. We should stress that, even if HAEBe stars were well-suited for interstellar extinction studies, as demonstrated earlier in this paper, our physical approach leads to a much less scattered extinction bump, also indicating that the discovery of variable peak positions by Blasberger et al. (2017) is questionable.

**4 SUMMARY**

We have determined the UV extinction curves for a sample of interstellar lines of sight toward 26 Herbig Ae/Be stars, by comparing the observed IUE spectrum with the Kurucz stellar model atmospheric spectrum for each object. The extinction is represented by an analytical formula consisting of a linear background, a Drude function for the extinction bump, and a FUV nonlinear rise. It is found that, peaking at  $\sim 2200 \text{ \AA}$ , the peak positions of the extinction bumps are rather stable and the scatters are small. This is consistent with the conventional wisdom that while the strength and width of the interstellar extinction bump vary with environment, its central wavelength is quite invariant.

**ACKNOWLEDGEMENTS**

We thank B.T. Draine, Q. Li, Q. Lin and the anonymous referee for valuable suggestions. QW and XJY are supported in part by NSFC 12122302 and 11873041. AL is supported in part by NASA grants 80NSSC19K0572 and 80NSSC19K0701.

**DATA AVAILABILITY**

The data underlying this article will be shared on reasonable request to the corresponding authors.

**REFERENCES**

- Alecian, E., Wade, G. A., Catala, C., et al. 2013, *MNRAS*, 429, 1001
- Blasberger, A., Behar, E., Perets, H. B., Brosch, N., & Tielens, A. G. G. M. 2017, *ApJ*, 836, 173
- Boersma, C., Peeters, E., Martín-Hernández, N. L., et al. 2009, *A&A*, 502, 175
- Cardelli, J. A., Clayton, G. C., & Mathis, J. S. 1989, *ApJ*, 345, 245
- Castelli, F., & Kurucz, R. L. 2004, arXiv:0405087
- Chhowalla, M., Wang, H., Sano, N., Teo, K. B., Lee, S. B., & Amaratunga, G. A. 2003, *Phys. Rev. Lett.*, 90, 155504
- Decleir, M., Gordon, K. D., Andrews, J. E., et al. 2022, *ApJ*, 930, 15
- Draine, B.T. 1988, *ApJ*, 333, 848
- Draine, B.T. & Malhotra, S. 1993, *ApJ*, 414, 632
- Fairlamb, J. R., Oudmaijer, R. D., Mendigutá, I., Ilee, J. D., & van den Ancker, M. E. 2015, *MNRAS*, 453, 976
- Fitzpatrick, E. L., & Massa, D. 1986, *ApJ*, 307, 286
- Fitzpatrick, E. L., & Massa, D. 1988, *ApJ*, 328, 734
- Garrison, L. M. 1978, *ApJ*, 224, 535
- Gordon, K. D., Clayton, G. C., Decleir, M., et al. 2023, arXiv:2304.01991
- Hamaguchi, K., Yamauchi S., & Koyama K. 2005, *ApJ*, 618, 360
- Hernández, J., Calvet, N., Hartmann, L., et al. 2005, *AJ*, 129, 856
- Iglesias-Groth, S., Ruiz, A., Bretón, J., & Gomez Llorente, J. M. 2003, *J. Chem. Phys.*, 118, 7103
- Joblin, C., Léger, A., & Martin, P. 1992, *ApJ*, 393, L79
- Lamers, H. J. G. L. M., Snow, T. P., & Lindholm, D. M. 1995, 455, 269
- Li, A., & Draine, B. T. 2001, *ApJ*, 554, 778
- Li, A., & Lunine, J.I. 2003, *ApJ*, 594, 987
- Li, A., Chen, J.H., Li, M.P., Shi, Q.J., & Wang, Y.J. 2008, *MNRAS*, 390, L39
- Ma, X.Y., Zhu, Y.Y., Yan, Q.B., You, J.Y., & Su, G. 2020, *MNRAS*, 497, 2190
- Massa, D., Gordon, K. D., & Fitzpatrick, E. L. 2022, *ApJ*, 925, 19
- Mathis, J.S. 1994, *ApJ*, 422, 176
- Ruiz, A., Bretón, J., & Gomez Llorente, J. M. 2005, *Phys. Rev. Lett.*, 94, 105501
- Schild, R. E. 1978, *ApJ*, 37, 77
- Seok, J. Y. & Li, A. 2017, *ApJ*, 835, 291
- Sheng X.L., Yan Q.B., Ye F., Zheng Q.R., & Su G. 2011, *Phys. Rev. Lett.*, 106, 155703
- Stecher, T. P. 1965, *ApJ*, 142, 1683
- Stecher, T. P. & Donn, B. 1965, *ApJ*, 142, 1681
- Steglich, M., Jäger, C., Huisken, F., et al. 2013, *ApJS*, 208, 26
- Valencic, L. A., Clayton, G. C., & Gordon, K. D. 2004, *ApJ*, 616, 912
- Verhoeff, A.P., Waters, L.B.F.M., van den Ancker, M.E., et al. 2012, *A&A*, 538, A101
- Whittet, D.C B. 2022, *Dust in the Galactic Environment* (3rd Edition), Bristol: IOP Publishing
- Witstok, J., Shivaie, I., Smit, R., et al. 2023, *Nature*, in press (arXiv:2302.05468)
- Witt, A. N., & Cottrell, M. J. 1980, *ApJ*, 235, 899

This paper has been typeset from a  $\text{\TeX}$ / $\text{\LaTeX}$  file prepared by the author.

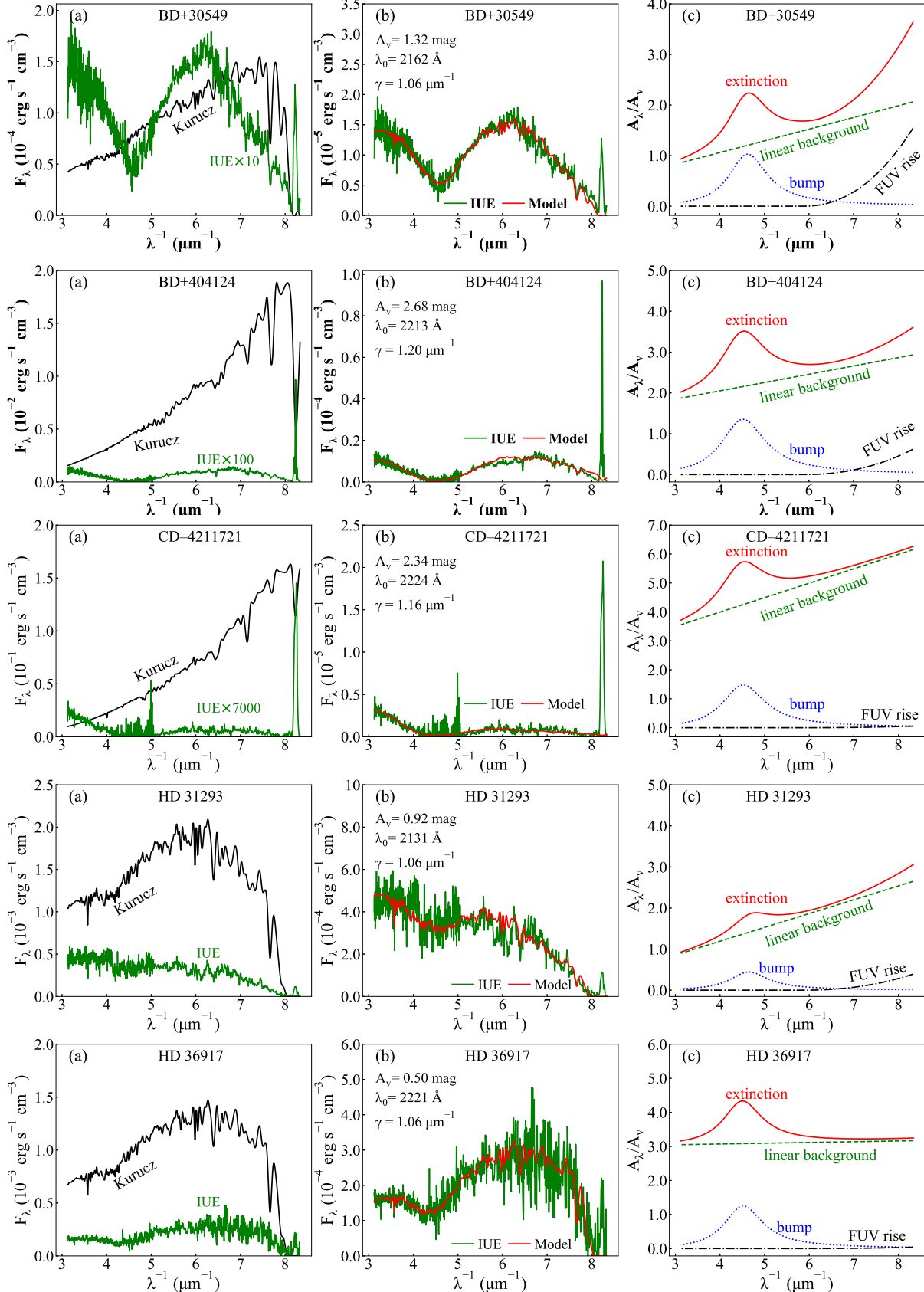


**Figure 1.** Observed, extinction-suffering IUE spectra ( $F_{\lambda}^{\text{obs}}$ ), “intrinsic”, extinction-free spectra ( $F_{\lambda}^{\text{int}}$ ), and UV extinction curves of the interstellar lines of sight toward BD+30549, BD+404124, CD-4211721, HD 31293, and HD 36917. The left columns compare  $F_{\lambda}^{\text{obs}}$  (green solid lines) with  $F_{\lambda}^{\text{int}}$  (black solid lines). The middle columns highlight the best fits (red solid lines) to the observed spectra (green solid lines). The right columns show the interstellar extinction curves expressed as  $A_{\lambda}/A_v$ . The red line is the FM parametrization at  $\lambda^{-1} > 3.3 \mu\text{m}^{-1}$ , which is the sum of a linear “background” (green line), a Drude bump of width  $\gamma$  peaking at  $x_0 \equiv \lambda_0^{-1}$  (blue line), and a nonlinear FUV rise (black dash-dotted line) at  $\lambda^{-1} > 5.9 \mu\text{m}^{-1}$ .

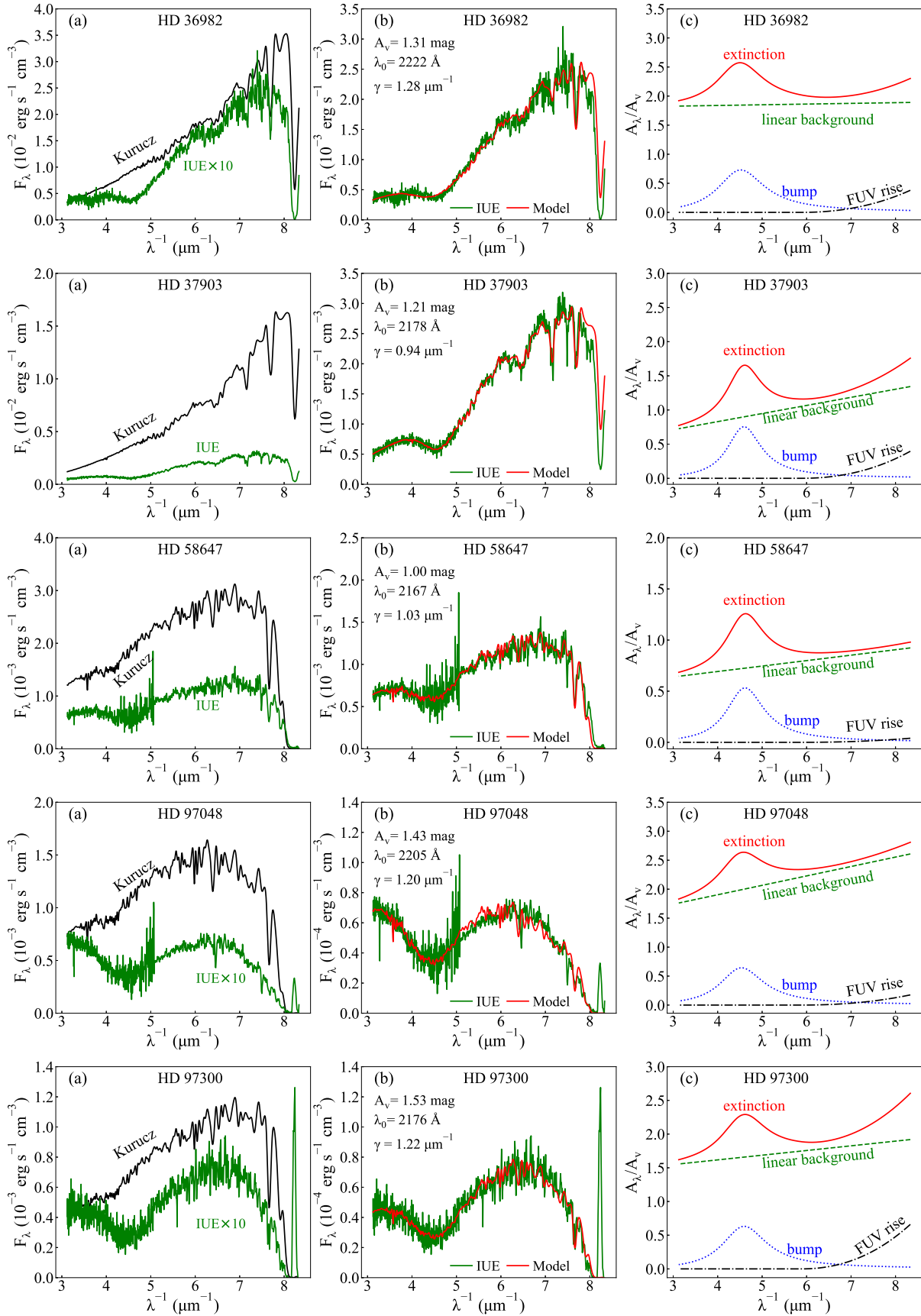


Figure 2. Same as Figure 1 but for HD 36982, HD 37903, HD 58647, HD 97048, and HD 97300

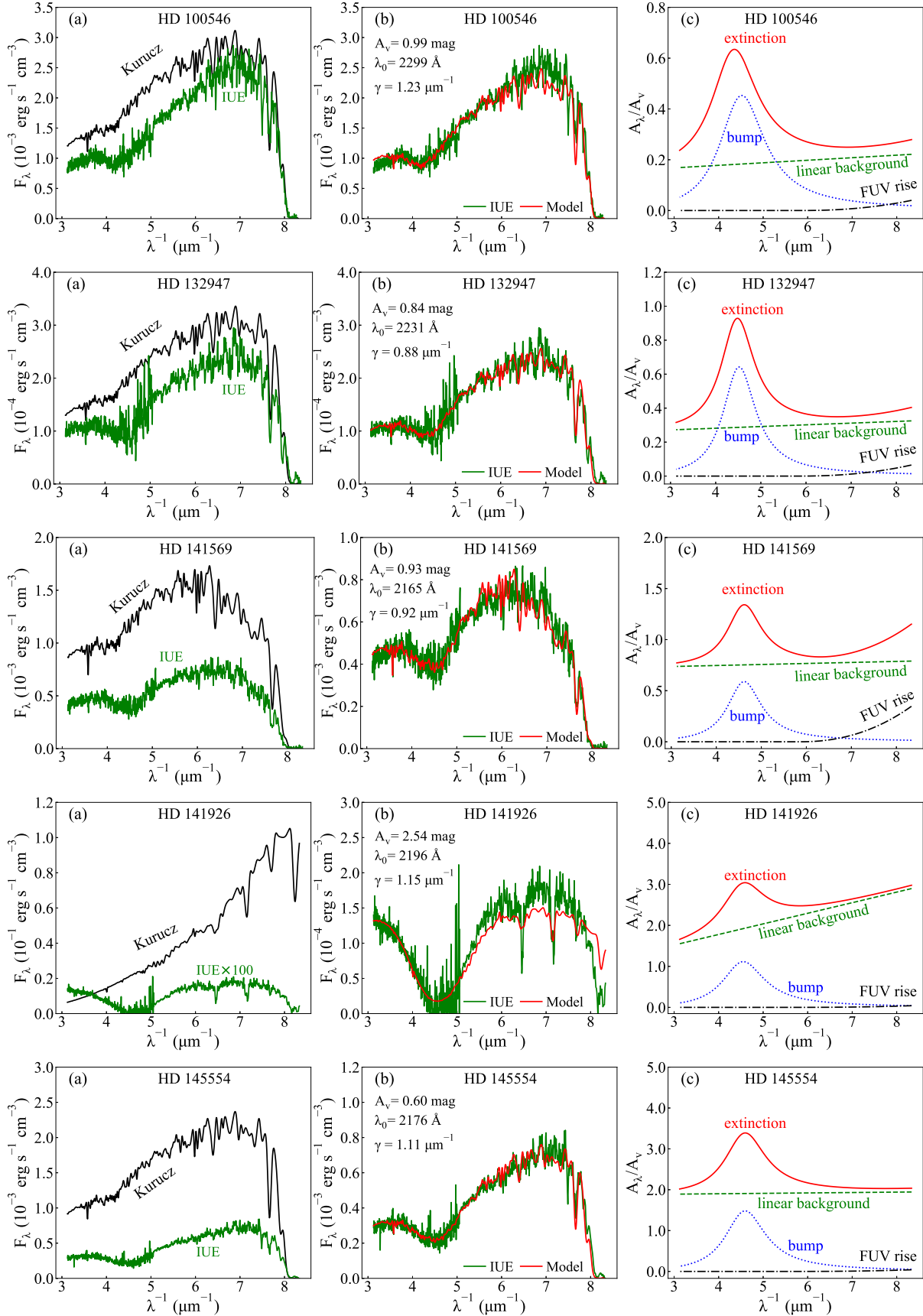


Figure 3. Same as Figure 1 but for HD 100546, HD 132947, HD 141569, HD 141926, and HD 145554.

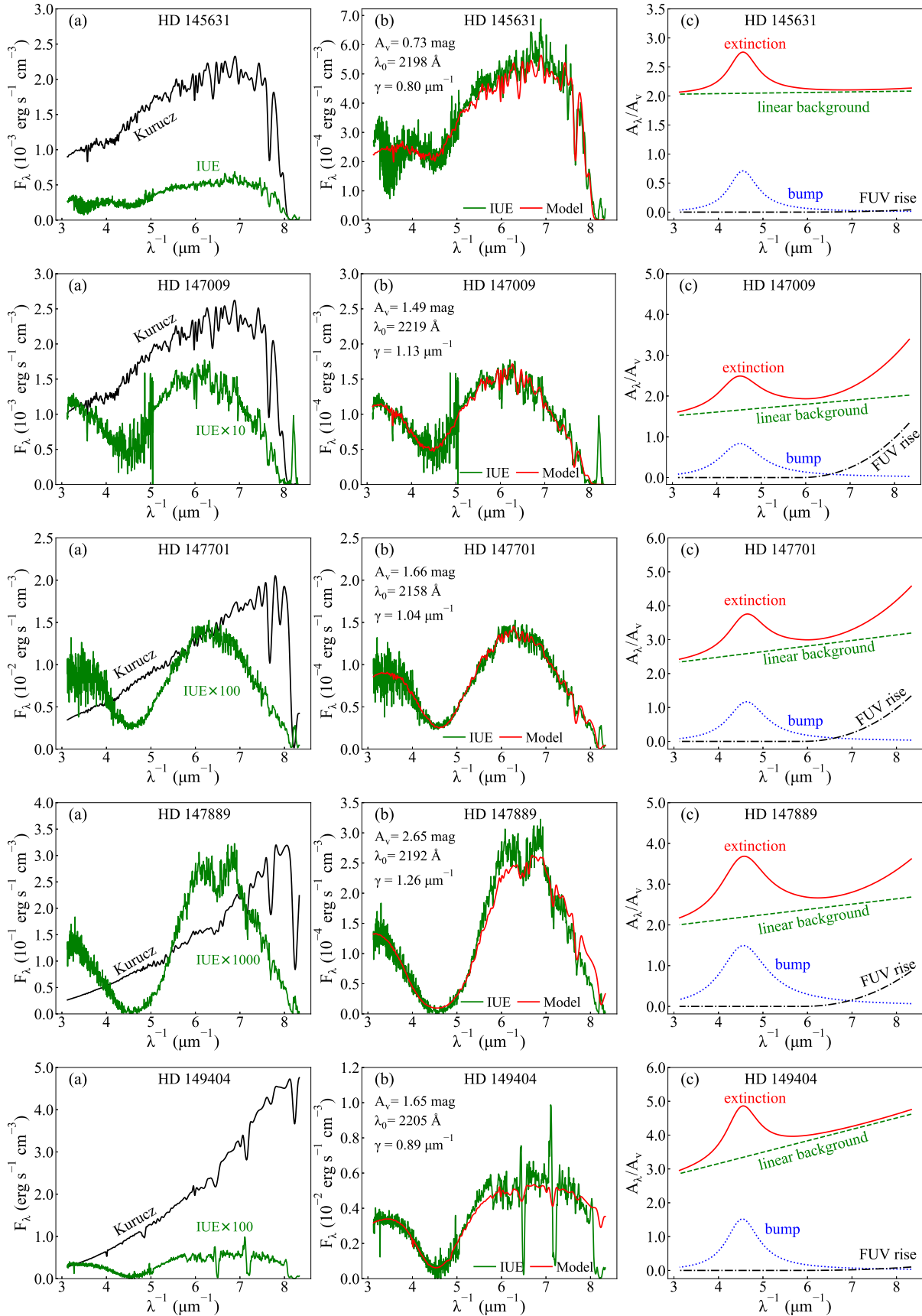


Figure 4. Same as Figure 1 but for HD 145631, HD 147009, HD 147701, HD 147889, and HD 149404.



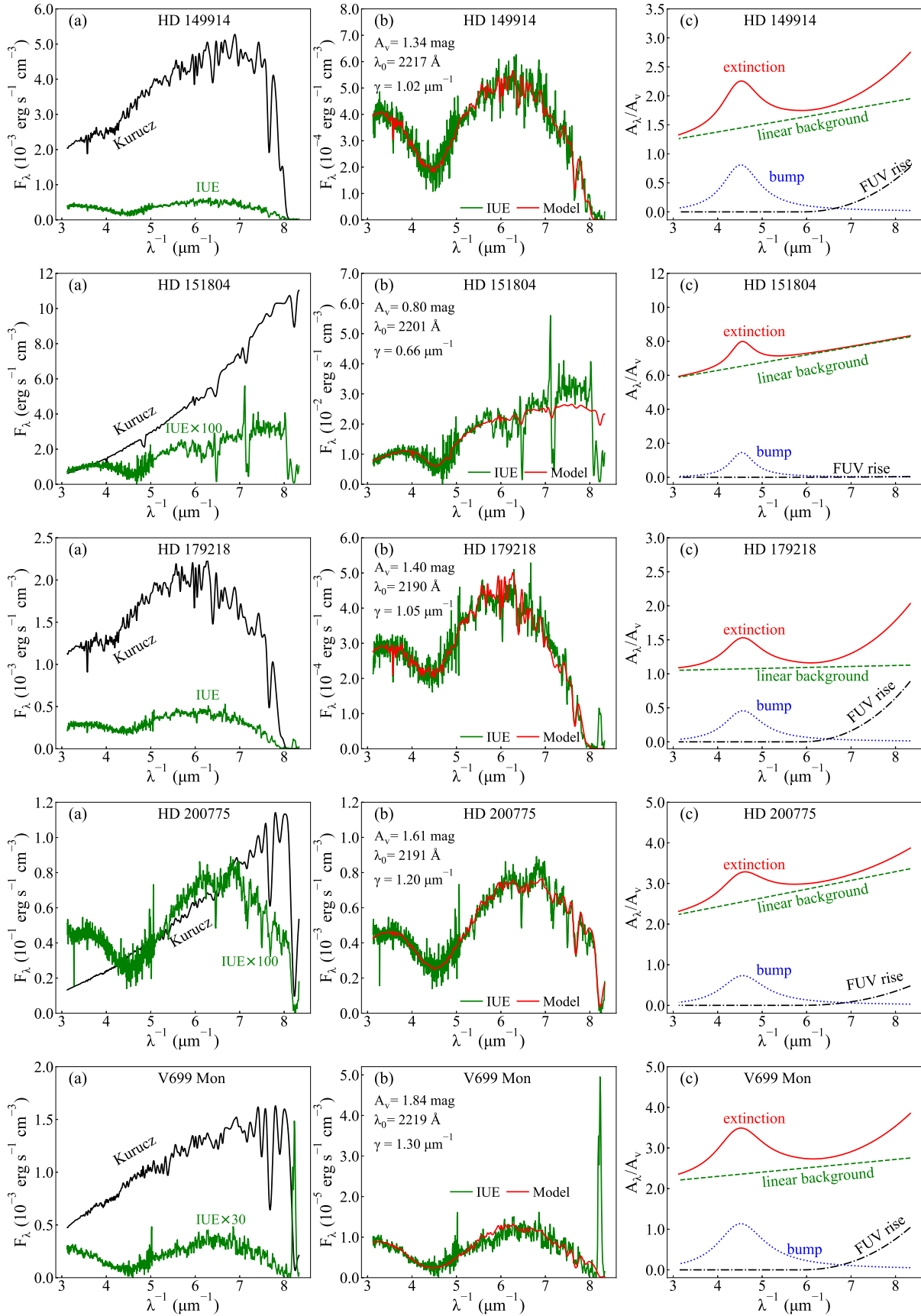


Figure 5. Same as Figure 1 but for HD 149914, HD 151804, HD 179218, HD 200775, and V699 Mon.

**Table 1.** Stellar Parameters

Object	Spectral Type <sup>†</sup>	E(B-V) <sup>†</sup> (mag)	$T_{\text{eff}}$ (K)	$L_*/L_{\odot}$	Distance (pc)	Stellar Radius (cm)	$R_*/R_{\odot}$	References <sup>‡</sup>
BD+30549	B8:p	0.59	12022	12.59	350	5.67E+10		(6)
BD+404124	B2Ve	0.98	22000	5900	980	3.67E+11		(1)
CD-4211721	B0IVe	1.58	30000	8710	400	2.39E+11		(5)
HD 31293	A0Ve	0.13	9800	57.5	144	1.83E+11	2.62	(3)
HD 36917	B9III/IV	0.17	10000	245.5	375	3.62E+11		(1)
HD 36982	B1.5Vp	0.37	20000	1659.59	375	2.38E+11	3.42	(3)
HD 37903	B3IV	0.31	23677	3311.31	820	2.37E+11		(7)
HD 58647	B9IV	0.14	10500	912	546	6.33E+11		(1)
HD 95881	A1/A2III/IV	0.13	9000	7.6	118	7.91E+10		(1)
HD 97048	A0Vep	0.31	10000	44	150	1.53E+11		(1)
HD 97300	B9V	0.24	10700	37	188	1.23E+11		(1)
HD 100546	B9Vne	0.48	10500	32	103	1.19E+11		(1)
HD 132947	B9V	0.13	10500	93.3	565	2.02E+11	3.1	(4)
HD 141569	B9.5V	0.09	9800	30.9	116	1.34E+11		(1)
HD 141926	B2nne	0.74	28000	20118.7	1254	6.75E+11	9.7	(2)
HD 145554	B9V	0.20	10471	42.66	137	1.38E+11		(7)
HD 145631	B9V	0.20	10471	44.67	141	1.41E+11		(7)
HD 147009	A0V	0.28	10471	42.66	130	1.38E+11		(7)
HD 147701	B5III	0.71	15488	204.17	140	1.38E+11		(7)
HD 147889	B2III/IV	1.05	21877	1995.26	140	2.16E+11		(6)
HD 149404	O8.5Iab(f)p	0.69	32000		810	2.36E+12	33.9	(8)
HD 149914	B9.5IV	0.26	10471	128.82	159	2.39E+11		(7)
HD 151804	O8.5Iab(f)p	0.36	34000		580	2.36E+12	34	(8)
HD 179218	A0Ve	0.11	9640	182	254	3.35E+11		(1)
HD 200775	B2Ve	0.61	18600	8912.5	429	6.30E+11		(1)
V699 Mon	B7IIne	0.70	13800	616.6	800	2.99E+11	4.3	(2)

<sup>†</sup> Taken from Blasberger et al. (2017).

<sup>‡</sup> Seok & Li (2017), (2) Verhoeff et al. (2012), (3) Alecian et al. (2013), (4) Fairlamb et al. (2015), (5) Boersma et al. (2009), (6) Hamaguchi et al. (2005), (7) Hernández et al. (2005), (8) Lamers et al. (1995).

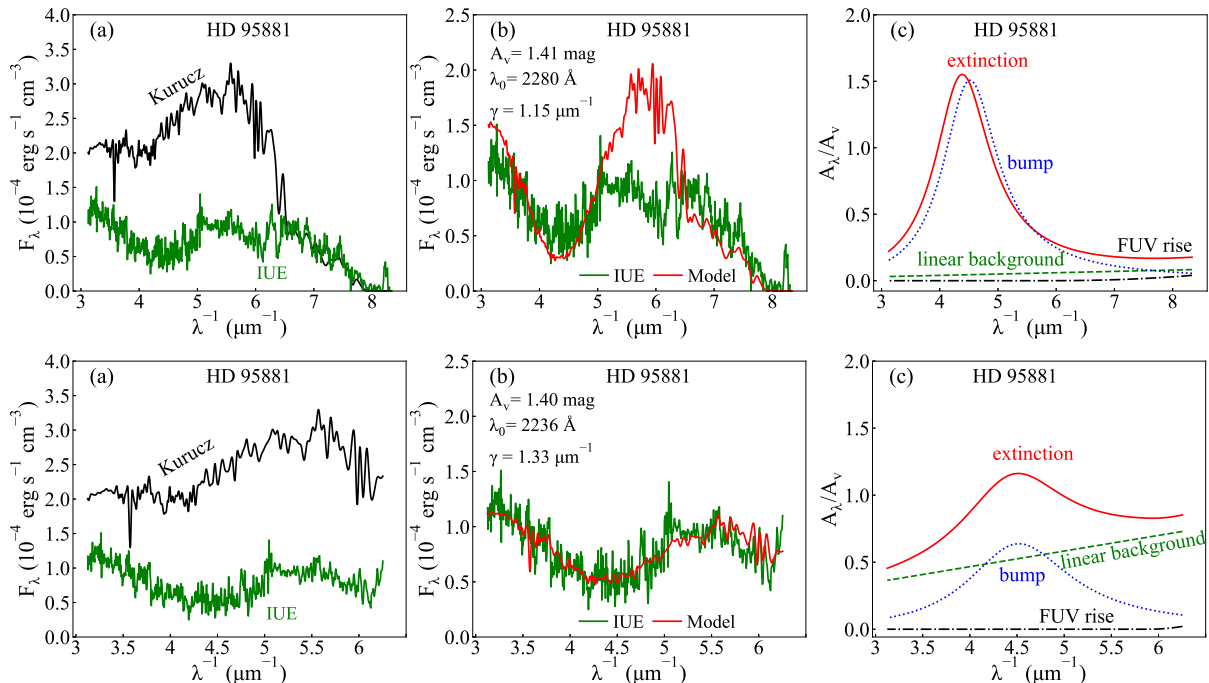


**Figure 6.** Same as Figure 1 but for the observed stellar and “intrinsic” spectra as well as the UV extinction curve of HD 95881 in the 1200–3200 Å wavelength range (upper panel) and in the 1600–3200 Å wavelength range (bottom panel).

**Table 2.** Extinction Model Parameters

Object	$A_V$ (mag)	$x_0$ (Å)	$\gamma$ ( $\mu\text{m}^{-1}$ )	$c_1$	$c_2$	$c_3$	$c_4$	$\chi^2$
BD+30549	1.32 ± 0.00	2161.7 ± 0.01	1.06 ± 0.01	0.14 ± 0.02	0.23 ± 0.00	1.15 ± 0.01	0.39 ± 0.03	6.39
BD+404124	2.68 ± 0.00	2213.2 ± 0.01	1.20 ± 0.02	1.24 ± 0.03	0.20 ± 0.01	1.95 ± 0.01	0.15 ± 0.11	157.25
CD-4211721	2.34 ± 0.00	2223.8 ± 0.01	1.16 ± 0.04	2.00 ± 0.14	0.50 ± 0.04	1.99 ± 0.02	0.01 ± 1.46	128.07
HD 31293	0.92 ± 0.00	2130.6 ± 0.03	1.06 ± 0.03	-0.15 ± 0.03	0.34 ± 0.01	0.50 ± 0.02	0.10 ± 0.04	13.87
HD 36917	0.50 ± 0.00	2221.3 ± 0.02	1.06 ± 0.02	2.98 ± 0.07	0.02 ± 0.01	1.40 ± 0.05	0.01 ± 0.04	6.82
HD 36982	1.31 ± 0.00	2222.2 ± 0.01	1.28 ± 0.01	1.79 ± 0.01	0.01 ± 0.00	1.20 ± 0.01	0.09 ± 0.01	6.48
HD 37903	1.21 ± 0.00	2177.8 ± 0.00	0.94 ± 0.01	0.36 ± 0.01	0.12 ± 0.00	0.66 ± 0.00	0.10 ± 0.01	1.72
HD 58647	1.00 ± 0.00	2166.8 ± 0.01	1.03 ± 0.01	0.48 ± 0.02	0.05 ± 0.00	0.57 ± 0.01	0.01 ± 0.01	6.13
HD 95881	0.65 ± 0.00	2244.2 ± 0.01	1.22 ± 0.01	-0.18 ± 0.05	0.31 ± 0.01	2.00 ± 0.03	0.01 ± 1.81	10.67
HD 97048	1.43 ± 0.00	2204.6 ± 0.01	1.20 ± 0.01	1.25 ± 0.02	0.16 ± 0.00	0.93 ± 0.01	0.04 ± 0.02	6.58
HD 97300	1.53 ± 0.00	2204.6 ± 0.01	1.22 ± 0.01	1.34 ± 0.01	0.07 ± 0.00	0.93 ± 0.01	0.16 ± 0.01	7.07
HD 100546	0.99 ± 0.01	2298.8 ± 0.02	1.23 ± 0.02	0.14 ± 0.02	0.01 ± 0.00	0.68 ± 0.01	0.01 ± 0.01	4.82
HD 132947	0.84 ± 0.01	2231.5 ± 0.01	0.88 ± 0.01	0.24 ± 0.02	0.01 ± 0.00	0.50 ± 0.01	0.02 ± 0.01	5.26
HD 141569	0.93 ± 0.00	2164.6 ± 0.01	0.92 ± 0.01	0.71 ± 0.02	0.01 ± 0.00	0.50 ± 0.01	0.09 ± 0.01	5.1
HD 141926	2.54 ± 0.00	2201.9 ± 0.00	1.17 ± 0.01	0.68 ± 0.03	0.28 ± 0.01	1.46 ± 0.01	0.01 ± 0.08	175.57
HD 145554	0.60 ± 0.00	2175.6 ± 0.01	1.11 ± 0.01	1.86 ± 0.03	0.01 ± 0.00	1.81 ± 0.02	0.01 ± 0.01	4.62
HD 145631	0.73 ± 0.00	2197.5 ± 0.02	0.80 ± 0.02	2.00 ± 0.04	0.01 ± 0.01	0.45 ± 0.02	0.01 ± 0.02	28.17
HD 147009	1.49 ± 0.00	2219.1 ± 0.01	1.13 ± 0.01	1.23 ± 0.02	0.10 ± 0.00	1.07 ± 0.01	0.33 ± 0.02	5.47
HD 147701	1.66 ± 0.00	2157.9 ± 0.01	1.04 ± 0.01	1.83 ± 0.01	0.16 ± 0.00	1.25 ± 0.01	0.34 ± 0.03	7.41
HD 147889	2.65 ± 0.00	2191.8 ± 0.01	1.26 ± 0.04	1.60 ± 0.02	0.13 ± 0.00	2.39 ± 0.01	0.22 ± 0.04	38.89
HD 149404	1.65 ± 0.00	2204.6 ± 0.00	0.89 ± 0.01	1.81 ± 0.02	0.34 ± 0.01	1.21 ± 0.01	0.03 ± 0.04	10.07
HD 149914	1.34 ± 0.00	2216.9 ± 0.01	1.02 ± 0.01	0.85 ± 0.01	0.13 ± 0.00	0.84 ± 0.01	0.19 ± 0.02	6.44
HD 151804	0.80 ± 0.00	2201.1 ± 0.01	0.66 ± 0.01	4.46 ± 0.04	0.46 ± 0.01	0.64 ± 0.01	0.01 ± 0.03	11.89
HD 179218	1.40 ± 0.00	2189.5 ± 0.01	1.05 ± 0.01	1.01 ± 0.01	0.01 ± 0.00	0.50 ± 0.01	0.22 ± 0.01	3.47
HD 200775	1.61 ± 0.00	2190.9 ± 0.01	1.20 ± 0.01	1.57 ± 0.01	0.22 ± 0.00	1.05 ± 0.01	0.12 ± 0.02	5.48
V699 Mon	1.84 ± 0.00	2219.2 ± 0.01	1.30 ± 0.01	1.88 ± 0.02	0.10 ± 0.00	1.92 ± 0.01	0.26 ± 0.03	13.17

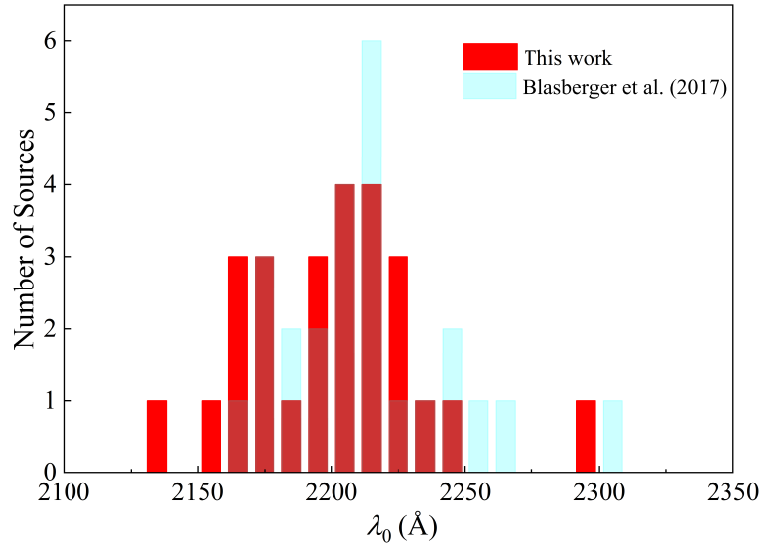


**Figure 7.** Histograms of the central wavelengths of the 2175 Å extinction bump for the 26 lines of sight determined in this work (red bars) as well as that derived by Blasberger et al. (2017; cyan bars).

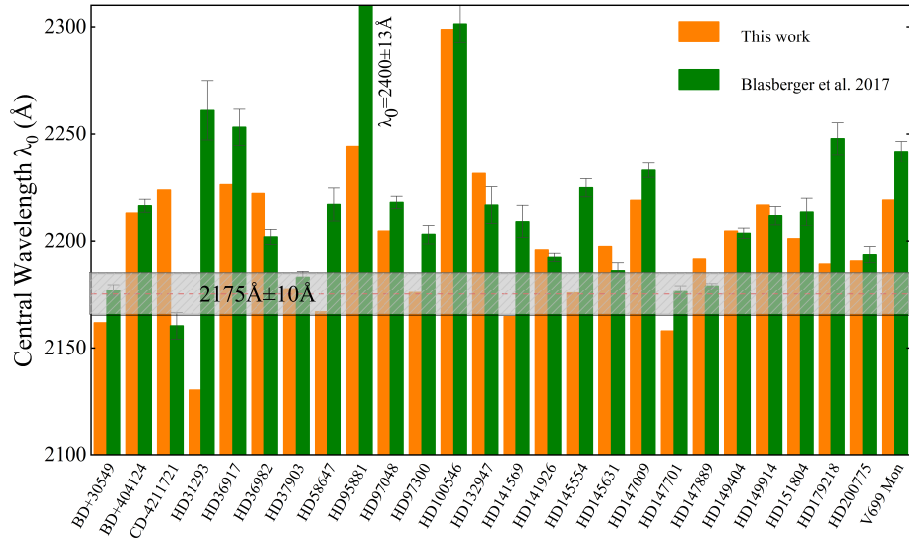


**Figure 8.** Comparison of the central wavelengths of the 2175 Å bump derived in this work (orange bars) with that determined by Blasberger et al. (2017; green bars). The horizontal bar shows the nominal wavelength of the 2175 Å extinction bump and its nominal variation range.

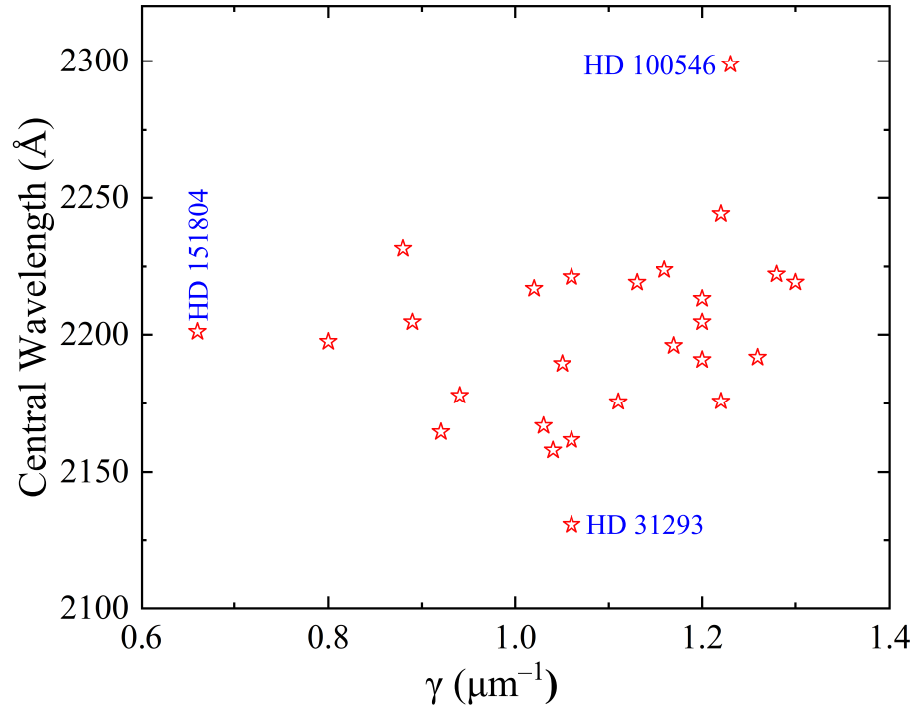


**Figure 9.** The central wavelength of the 2175 Å extinction bump against its width.